PRIFYSGOL BANGOR / BANGOR UNIVERSITY

PRIFYSGOL
BANGOR
UNIVERSITY

Effect of electric field on low temperature multisubband electron mobility in a coupled Ga0.5In0.5P/GaAs quantum well structure.

Sahu, T.; Shore, K.A.

Journal of Applied Physics

Cyswllt i'r cyhoeddiad / Link to publication

Effect of electric field on low temperature multisubband electron mobility in a coupled Ga 0.5 In 0.5 P / GaAs quantum well structure

Trinath Sahu and K. Alan Shore

Effect of electric field on low temperature multisubband electron mobility in a coupled Ga$_{0.5}$In$_{0.5}$P/GaAs quantum well structure

Trinath Sahu[1,a)] and K. Alan Shore[2]

[1]*Department of Electronic Science, Berhampur University, Berhampur 760 007, Orissa, India*
[2]*School of Electronic Engineering, Bangor University, Bangor, LL57 1UT, Wales, United Kingdom*

The effect of uniform electric field on low temperature (T=0 K) multisubband electron mobility μ_i is analyzed by considering a barrier delta-doped Ga$_{0.5}$In$_{0.5}$P/GaAs coupled double quantum well structure. We consider ionized impurity scattering and interface roughness (IR) scattering. The screening of the scattering potentials is obtained by adopting the random phase approximation. Starting with a double-subband occupied system we have studied the changes in the intrasubband and intersubband scattering processes by varying the electric field F and highlight the influence of F on the intersubband effects which yields interesting results on μ_i. At a certain electric field, the system undergoes a transition from double subband to single subband occupancy leading to a large enhancement in mobility due to the suppression of the intersubband interactions. We show that by reversing the electric field a large change in mobility is obtained due to the asymmetric nature of the IR scattering potential. It is also gratifying to show that by varying the electric field the relative dominance of different scattering mechanisms on subband mobility changes through the intersubband interaction. © *2010 American Institute of Physics*. [doi:10.1063/1.3391351]

I. INTRODUCTION

In recent years many attempts have been made to utilize electric field effects on coupled quantum well structures in developing electronic and optoelectronic devices. Novel functional quantum well devices have been fabricated by using the concept of resonant tunneling of electrons perpendicular to the interface planes.[1–3] Significant effort also been given utilizing coupled quantum wells or short period superlattices as quantum cascade lasers which have been shown to be reliable, compact, and high power optical sources in the midinfrared and terahertz frequency range.[4–6] The application of an electric field, perpendicular to the interface plane, changes the potential profile of a quantum well structure and thereby changes the subband energy levels. The subband wave function distributions also are amended thus affecting electron transport parallel to the interface plane. Basu and Raychaudhury[7] have studied the effect of electric field applied perpendicular to the layer plane in In$_{0.53}$Ga$_{0.47}$As/InP single quantum well structures and showed that increase in the electric field causes an increase in the scattering rate induced by the alloy disorder scattering. Lima *et al.*[8] have calculated the low temperature electron mobility in n-AlGaAs/GaAs/AlGaAs single asymmetric quantum wells in the presence of a uniform electric field perpendicular to the interface plane. They have shown that by changing the longitudinal electric field the electron wave function can be dislocated so that one can enhances the two-dimensional (2D) electron mobility. In the above work the electron mobility was studied by considering single quantum well structures in which only the lowest subband is occupied. Attempts have also been made to study carrier mobility in different quantum well structures by carrying out Monte Carlo

simulation.[9–12] However, to the best of our knowledge, the study of the effect of electric field on multisubband electron mobility, which very much relies on the intersubband interactions, has not previously been reported.

A double quantum well structure[13] exhibits the phenomenon of tunneling coupling in addition to quantum confinement effects. Double quantum well structures have been widely used not only to investigate the interesting physical phenomena of coupled 2D electron gas (2DEG) systems but also to fabricate novel electronic and optoelectronic devices.[14–16] In a double quantum well structure the subband electron wave functions of the individual wells overlap through a thin central barrier exhibiting splitting in the subband energy levels. By changing the well width, barrier width and carrier concentration, the subband energy levels change and hence for a certain set of values of the material parameters, the system undergoes transition from single subband occupancy to double subband occupancy. The electron transport in such multisubband occupied systems has been shown to be influenced by intersubband interactions.[17–22] In a recent paper[22] we studied the effect of intersubband interaction on the subband mobility of a coupled GaInP/GaAs double quantum well structure. We showed that the intersubband interaction not only controls the effect of roughness of different interfaces but also exhibits interesting results on the well width up to which the interface roughness (IR) dominates in a double quantum well structure.

In the present paper, we analyze the effect of the electric field perpendicular to the interface plane on the electron transport in a coupled double channel multisubband quantum well system. We consider a lattice matched GaInP/GaAs symmetric double quantum well structure. The low temperature electron mobility is assumed to be due to ionized impurity scattering and IR scattering. The screened scattering po-

---

a)Electronic mail: tsahu_bu@rediffmail.com.

107, 113708-1

tentials are obtained by using the random phase approximation (RPA) formalism.[17] We have considered a double subband occupied system and studied the effect of dislocation of the subband wave functions on the intrasubband and intersubband scattering rate matrix elements of different scattering mechanisms by changing the field strength. We show that the mobility increases with the electric field mainly due to the change in the intersubband scattering rate matrix elements. For a certain value of the electric field there is a cross over from double subband to single subband occupancy leading to a large enhancement in the mobility. This enhancement in mobility is due to the suppression of the intersubband effects. By reversing the electric field a large change in mobility occurs due to the asymmetric nature of the IR scattering potential. Normally in quantum wells having narrow widths, the mobility is dominated by IR scattering.[22–24] We show here that in the presence of an electric field the dominance of IR scattering on mobility persists in quantum wells of larger well widths. It will be of interest to compare our results with the experimental results when such are available.

II. THEORY

We consider a symmetric $GaAs/In_{0.5}Ga_{0.5}P$ double quantum well structure with a thin central barrier (InGaP) of width b ($-b/2 \le z \le b/2$). The adjacent wells are of width w. The outer barriers are delta-doped with Si at a distance s from the adjacent wells. The doping layer width and doping concentration are d and N_0, respectively. The barrier height V_b at the interfaces is taken as the conduction band offset of the InGaP layer and the GaAs layer. Two symmetric triangularlike potential wells in the GaAs layers near the interfaces with the outer barriers are formed due to Coulomb interaction between the ionized impurities in the barrier and the diffused electrons in the wells and also alignment of the Fermi level (E_F) throughout the system. The electrons are thus confined to two narrow strips forming two sheets of 2DEG (Ref. 17) coupled through a thin central barrier.

The electron subband wave functions and the energy eigenvalues for the 2D system can be obtained as[17]

$$\psi_{ik}(\vec{r}) = \frac{e^{i\vec{k}\cdot\vec{\rho}}}{\sqrt{A}}\psi_i(z) \tag{1}$$

and

$$E_{ik} = E_i + \frac{\hbar^2 k^2}{2m^*}, \tag{2}$$

where $\vec{\rho}$ is the 2D position vector parallel to the interface plane (xy-plane) and $\vec{k}$ is the corresponding wave vector. A is the area of the sample perpendicular to the z-axis and m^* the electron effective mass. E_i is the subband energy level, $i = 0, 1, 2, 3, ..$ being the subband index. In the presence of a longitudinal electric field, parallel to the z-direction, the envelope function $\psi_i(z)$ satisfies the one-dimensional Schrodinger equation,

$$\left[\frac{-\hbar^2}{2m^*}\frac{d^2}{dz^2} + V(z) + eFz\right]\psi_i(z) = E_i\psi_i(z), \tag{3}$$

where F is the electric field strength. The Hartree potential $V(z)$ which causes band bending due to the electrostatic interaction of the electrons and the ionized impurities, is obtained by solving Poisson's equation

$$\frac{d^2V}{dz^2} = \frac{4\pi e^2}{\epsilon_o}[n_D(z) - n(z)], \tag{4}$$

where ϵ_o is the dielectric constant of the layer, $n_D(z)$ and $n(z)$ are the impurity and electron concentration distributions, respectively,

$$n_D(z) = N_0 \quad b/2 + w + s < |z| < b/2 + w + s + d$$

$$= 0 \quad \text{otherwise}$$

$$n(z) = \sum_i n_i |\psi_i(z)|^2 \quad -\infty < z < +\infty, \tag{5}$$

where n_i is the number of electrons per unit area in the ith subband

$$n_i = \left(\frac{m^* k_B T}{\pi \hbar^2}\right)\ln[1 + e^{(E_F - E_i)/k_B T}], \tag{6}$$

where E_F is the Fermi energy. At T=0, the surface electron density $N = 2N_o d$ is related to the Fermi energy through n_i as

$$N = \sum_{i=1}^{p} n_i \theta(E_F - E_i), \tag{7}$$

where p is the number of filled levels, θ is the heaviside step function.

We obtain an expression for $V(z)$ by solving the Poisson's equation with the use of a trial wave function and adopting the variational formalism.[17] We use electrostatic boundary conditions at the interfaces and the condition that the electrostatic potential remains constant (V_b/e) and the electric field vanishes at the extremes of the structure. We also incorporate the conduction band discontinuity at the interfaces. We obtain an analytical expression for the potential profile as a function of the electric field and calculate the transmission coefficient through the potential profile by adopting the multistep potential approximation[25] to numerically calculate the bound subband energy levels E_i, wave functions ψ_i and subband electron density n_i.

The electron mobility μ can be written as $1/\mu = \Sigma_s 1/\mu^s$, where s denotes the different scattering mechanisms. We consider that the low temperature mobility is governed by IR scattering and ionized impurity scattering. μ^s is defined by the subband transport mobility μ_i^s as

$$\mu^s = \frac{\Sigma_i n_i \mu_i^s}{\Sigma_i n_i}. \tag{8}$$

Further, the subband transport mobility μ_i^s and subband transport life time τ_i^s of an electron in the ith subband is given by

$$\mu_i^s(\epsilon) = \frac{e}{m^*}\tau_i^s(\epsilon). \qquad (9)$$

At T=0 K the electrons on the Fermi surface contribute to electron transport. Therefore we have $\tau_i^s = \tau_i^s(E_{Fi})$, where $E_{Fi}=E_F-E_i$ is the Fermi level in the ith subband. In general, for a multisubband system the expressions for μ_i^s are difficult to interpret as they are comprised of intrasubband and intersubband scattering processes in a mixed way. However, for a single occupied subband (i=0), one can obtain[18,20]

$$\frac{1}{\tau_0^s} = B_{00}^s. \qquad (10)$$

The intrasubband scattering rate matrix element B_{ii}^s is given by the scattering matrix elements $V_{ii}^s(q)$ as

$$B_{ii}^s = \frac{m}{\pi\hbar^3}\int_0^\pi d\theta(1-\cos\theta)|V_{ii}^s(q_{ii})|^2, \qquad (11)$$

where $q_{ii}=2k_{Fi}\sin\theta/2$. Similarly the expressions for τ_i^s for a system with double occupied subbands can be obtained by taking i=0 and 1 as[18,20]

$$\frac{1}{\tau_0^s} = \frac{(B_{00}^s + C_{01}^s)(B_{11}^s + C_{10}^s) - D_{01}^s D_{10}^s}{(B_{11}^s + C_{10}^s) + (E_{F1}/E_{F0})^{1/2}D_{01}^s} \qquad (12)$$

and

$$\frac{1}{\tau_1^s} = \frac{(B_{00}^s + C_{01}^s)(B_{11}^s + C_{10}^s) - D_{01}^s D_{10}^s}{(B_{00}^s + C_{01}^s) + (E_{F0}/E_{F1})^{1/2}D_{10}^s}, \qquad (13)$$

where C_{ij}^s and D_{ij}^s are intersubband scattering rate matrix elements.

$$C_{ij}^s = \frac{m}{\pi\hbar^3}\int_0^\pi d\theta|V_{ij}^s(q_{ij})|^2, \qquad (14)$$

$$D_{ij}^s = \frac{m}{\pi\hbar^3}\int_0^\pi d\theta\cos\theta|V_{ij}^s(q_{ij})|^2. \qquad (15)$$

Here $q_{ij}=(k_{Fi}^2+k_{Fj}^2-2k_{Fi}k_{Fj}\cos\theta)^{1/2}$. For screened ionized impurity scattering, V_{ij}^s can be written as[19,20]

$$|V_{ij}^{imp}(q)|^2$$
$$= \frac{4\pi^2 e^4 N_0}{\epsilon_0^2 q^2}$$
$$\times \left[\int_{-(b/2+w+s+d)}^{-(b/2+w+s)} dZ \left|\sum_{i'j'}\epsilon_{ij,i'j'}^{-1}(q)P_{i'j'}(q,Z)\right|^2\right.$$
$$\left.+ \int_{(b/2+w+s)}^{(b/2+w+s+d)} dZ \left|\sum_{i'j'}\epsilon_{ij,i'j'}^{-1}(q)P_{i'j'}(q,Z)\right|^2\right], \qquad (16)$$

where

$$P_{i'j'}(q,Z) = \int_{-\infty}^{\infty} dz\psi_{i'}(z)\psi_{j'}(z)e^{-q|z-Z|}, \qquad (17)$$

where Z is the z-component of the position vector of the impurity layer, $\epsilon_{ij,i'j'}^{-1}$ is the elements of the inverse matrix of the dielectric function, and i,j,i',j' are subband indices. The sum over i' and j' runs over all the subband levels of the system. Within the RPA the dielectric function matrix can be written as

$$\epsilon_{ij,i'j'}(q) = \delta_{ii'}\delta_{jj'} + (q_s/q)f_{ij,i'j'}(q)\chi_{i'j'}^0(q), \qquad (18)$$

where $q_s=2me^2/\epsilon_0\hbar^2$ and f is the Coulomb form factor and $\chi_{i'j'}^0(q)$ is the static electron density-density correlation function without electron-electron interaction.[17] For screened IR scattering potential, we consider an expression appropriate for a finite well of height V_0 (Refs. 26–28)

$$|V_{ij}^{IR}(q)|^2 = \sum_I V_0^2\pi\Delta_I^2\Lambda_I^2 e^{-q^2\Lambda_I^2/4}$$
$$\times \left|\sum_{i'j'}\epsilon_{ij,i'j'}^{-1}(q)\psi_{i'}^*(z)\psi_{j'}(z)_{|z=z_I}\right|^2, \qquad (19)$$

since the corresponding equation for an infinite well, given by Prange and Nee,[29] has been shown to be not very accurate.[27] In the above equation, Δ_I is the mean height and Λ_I is the correlation length of the roughness of the Ith interface at $z=z_I$. We consider the scattering of impurities from the two δ-doped layers in the outer barriers. In the case of IR scattering, basing upon experimental evidence, the interfaces lying on the substrate side of the wells are assumed to be significant.[30–32] We thus consider the scattering from the first (I_1) and third (I_3) interfaces, say, from left of the structure, i.e., $z_1=-(b/2+w)$ and $z_3=b/2$. We assume that the interfaces are equally rough.

III. RESULTS AND DISCUSSION

We calculate the subband electron mobility μ_i in a GaInP/GaAs double quantum well structure by changing the strength of the uniform applied electric field F (in kV/cm). We consider a typical case in which the two lowest subbands are occupied by taking well width $w=100$ Å. The other parameters of the structure are: $b=20$ Å, $s=80$ Å, $d=20$ Å, $N_0=1\times10^{18}$ cm^{-3}, and $N_s=4\times10^{11}$ cm^{-2}. The effective mass of the electron m^* (in m_0) and the static dielectric constant ϵ_0 for GaAs/GaInP are 0.067/0.092 and 13.18/11.8, respectively. The barrier height $V_b=130$ meV and the IR parameters $\Delta=5.67$ Å and $\Lambda=140$ Å.[33] Our aim is to analyze
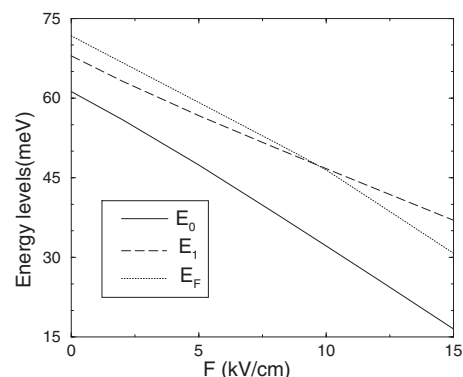

FIG. 1. Subband energy levels E_0 and E_1 and Fermi energy level E_F in meV as a function of electric field F in kV/cm along the negative z-axis. At $|F|$ =10 kV/cm transition from double subband occupancy to single subband occupancy is exhibited.
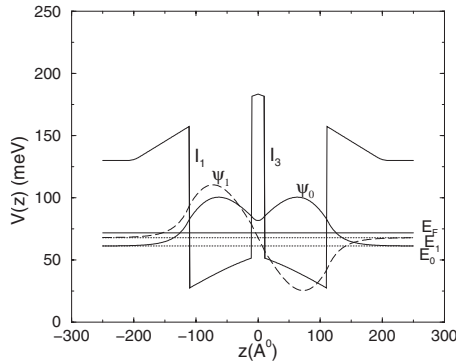
FIG. 2. Schematic subband wave functions $\psi_0(z)$ (solid curve) and $\psi_1(z)$ (dashed curve), subband energy levels, E_0 and E_1 and Fermi energy level E_F for the potential profile $V(z)$ (in meV) as a function of z (in Å) with $F=0$.

FIG. 4. Schematic subband wave functions $\psi_0(z)$ (solid curve) and $\psi_1(z)$ (dashed curve), subband energy levels, E_0 and E_1 and Fermi energy level E_F for the potential profile $V(z)$ (in meV) as a function of z (in Å) with $F=+15$ kV/cm showing displacement of subband wave functions compared to that of $F=0$.

the effect of the electric field on the intra- and intersubband scattering rates mediated by intersubband interactions.

In Fig. 1, we plot the results of E_0, E_1, and E_F (meV) as a function of the electric field F (kV/cm) perpendicular to the interface plane and directed along the negative z-axis. A change from double-to-single subband occupancy occurs as F increases from 9 to 10 kV/cm. By reverting the field F along z-axis, the magnitudes of E_0, E_1, and E_F change. However, the subband Fermi energy $E_{Fi}=(E_F-E_i)$ (meV) remains invariant because of the symmetric nature of the potential profile of the structure at $F=0$ (Fig. 2). In Figs. 2–4 we plot $V(z)$, E_i, and $\psi_i(z)$ as a function of z for $F=0$, -15 (kV/cm), and $+15$ (kV/cm), respectively. These figures illustrate the schematic changes in the distributions of $\psi_i(z)$ due to F relative to the interface planes (I_1 and I_3) and the delta-doped layers (lying at $\pm(b/2+w+s)$) which effect the scattering potentials.

In Figs. 5 we present the variation in both μ_i^{imp} and μ_i^{IR} (cm^2/V s) with increase in F (kV/cm) along the negative z-axis. As long as two subbands are occupied, $\mu_i^{imp/IR}$ is due to the mixed contributions of intrasubband ($B_{ii}^{imp/IR}$) and intersubband ($C_{01}^{imp/IR}$ and $D_{01}^{imp/IR}$) scattering rate matrix elements. In Figs. 6 and 7, we plot $B_{00}^{imp/IR}$, $B_{11}^{imp/IR}$, $C_{01}^{imp/IR}$, and $D_{01}^{imp/IR}$ to illustrate the dependence of $\mu_i^{imp/IR}$ on the electric field in Fig. 5. As F increases E_{F1} decreases and becomes
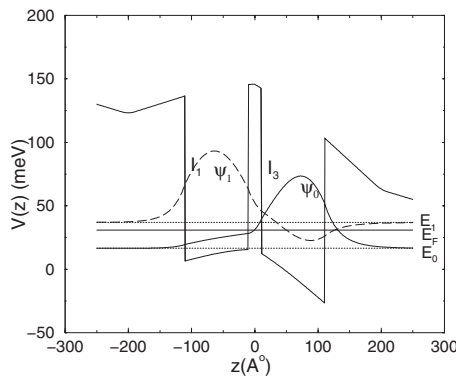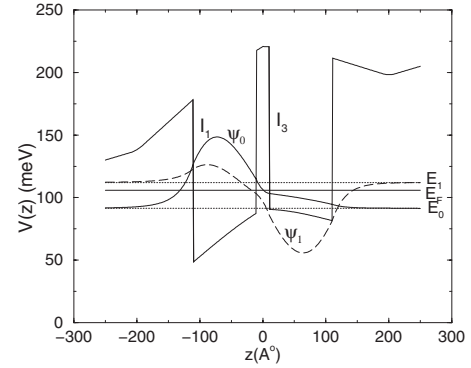
almost zero near $|F|=9$ kV/cm (Fig. 1). This leads to a sharp enhancement in B_{11}^{imp} (the value of B_{11}^{imp} near $|F|=9$ kV/cm could not be shown in Fig. 6 as it is beyond the scale) thereby reducing μ_1^{imp} to zero (Fig. 5). However, no such singularity is observed in B_{11}^{IR} (Fig. 7). The variation in B_{11}^{IR} mainly depends upon the changes in the amplitudes of $\psi_0(z)$ and $\psi_1(z)$ at the interface planes I_1 and I_3 mediated by the dielectric screening matrix. Regarding the variation in $B_{00}^{imp/IR}$ in Figs. 6 and 7, a sudden drop in B_{00}^{imp} occurs near $|F|=9$ kV/cm while B_{00}^{IR} exhibits a monotonic decreasing trend with increase in F. In the expression for B_{00}^{imp}, the integrand in the right hand side of Eq. (11) contains $(1-\cos\theta)$ which cancels with the q^2 factor occurring in the denominator of $|V_{00}^{imp}(q)|^2$ (Eq. (16)). Therefore the drop in B_{00}^{imp} is mainly due to the discontinuity of the inverse dielectric screening function matrix near the transition from the double subband occupancy to single subband occupancy.[22] However, in the case of B_{00}^{IR} there is no such cancellation. Hence the occurrence of the weight factor $(1-\cos\theta)$ in the integrand almost compensates the change in the dielectric screening matrix resulting a monotonic decrease in B_{00}^{IR}.

From Figs. 6 and 7, we further note that for small F, the intersubband scattering rate matrix elements $C_{01}^{imp/IR}$ and $D_{01}^{imp/IR}$ are dominant. Therefore the largest contribution to subband mobility $\mu_i^{IR/imp}$ (in Fig. 5) mainly derives from the intersubband interaction terms, i.e., $C_{01}^{imp/IR}$ and $D_{01}^{imp/IR}$. As
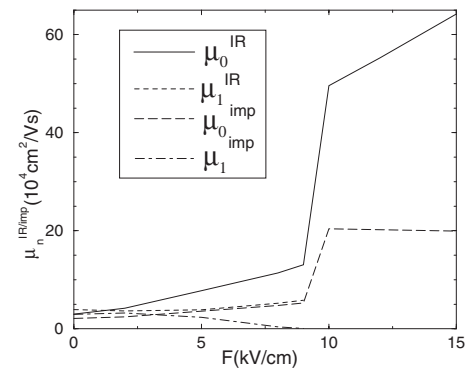

FIG. 3. Schematic subband wave functions $\psi_0(z)$ (solid curve) and $\psi_1(z)$ (dashed curve), subband energy levels, E_0 and E_1 and Fermi energy level E_F for the potential profile $V(z)$ (in meV) as a function of z (in Å) with $F=-15$ kV/cm showing the displacement of subband wave functions compared to that of with $F=0$.

FIG. 5. Subband mobility μ_i^{imp} and μ_i^{IR} in 10^4 cm^2/V s as a function of F along the negative z-axis.
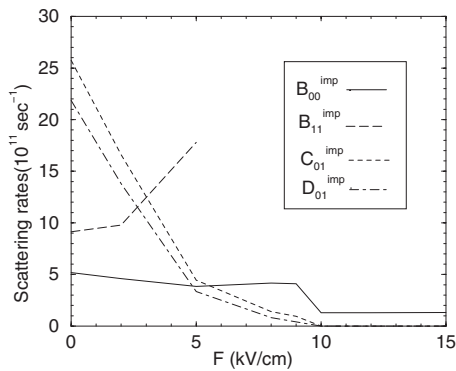
FIG. 6. Scattering rate matrix elements B_{00}^{imp}, B_{11}^{imp}, C_{01}^{imp}, and D_{01}^{imp} in 10^{11} s^{-1} as a function of F along the negative z-axis. With increase in F, C_{01}^{imp} and D_{01}^{imp} decrease sharply.

FIG. 8. Subband mobility μ_i^{imp} and μ_i^{IR} in 10^4 cm^2/V s as a function of F along z-axis.

$|F|$ increases both $C_{01}^{imp/IR}$ and $D_{01}^{imp/IR}$ first decrease sharply and then slowly because of the change in the overlapping of $\psi_0(z)$ and $\psi_1(z)$. For $|F| > 5$ kV/cm, μ_0^{imp} is dominated by the intrasubband scattering rate B_{00}^{imp}. Whereas, μ_0^{IR} is dominated by C_{01}^{IR} up to $F = 9$ kV/cm, i.e., for the entire range of double subband occupancy. The large increase in μ_0^{imp} (in Fig. 5) is due to the sudden drop in B_{00}^{imp} (Fig. 6), while that of μ_0^{IR} (Fig. 5) is due to suppression of C_{01}^{IR} and D_{01}^{IR} (Fig. 7) i.e., the intersubband interaction during the transition to single subband occupancy.

In Fig. 8, we present the variation in $\mu_i^{imp/IR}$ (cm^2/V s) with F (kV/cm) along the positive z-axis and compare that in Fig. 5 where F is directed along the negative z-axis. We note that in both the cases the magnitudes of μ_i^{imp} remain unchanged. This is because the effect of ionized impurity scattering on the subband electrons is from the ionized donors lying in two delta-doped layers symmetrically placed in the side barriers. Therefore the net effect of the scatterers remains invariant with the direction of the electric field. However, in the case of μ_i^{IR}, the IR scattering potential is considered to be due to the interfaces (I_1 and I_3) lying toward the substrate side of the structure.[30–32] Therefore μ_i^{IR} differs according to the direction of the electric field F. As $|F|$ varies from 0 to 9 kV/cm, μ_0^{IR} remain almost unchanged in Fig. 8, while it becomes about four times larger in Fig. 5.

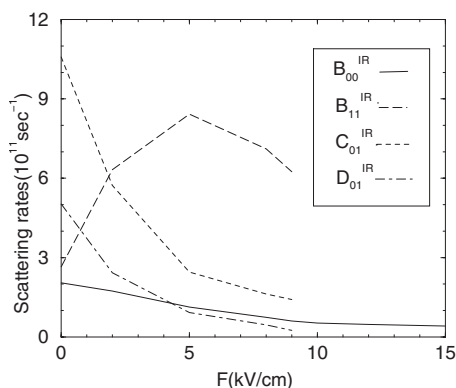In Fig. 9, we plot B_{00}^{IR}, B_{11}^{IR}, C_{01}^{IR}, and D_{01}^{IR} as functions of
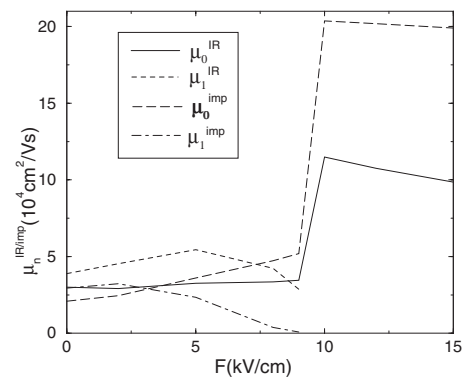
F along the positive z-axis. The change in μ_0^{IR} in Figs. 5 and 8, is attributed to the changes in C_{01}^{IR} and B_{00}^{IR} in Figs. 7 and 9, respectively.

In order to calculate the electron mobility μ, we first calculate the mobility limited by the ionized impurity scattering μ^{imp} and IR scattering μ^{IR} by using Eq. (8). The mobility is then calculated using the relation $1/\mu = 1/\mu^{imp} + 1/\mu^{IR}$ and plotted in Figs. 10 and 11 for F along the negative z-axis and positive z-axis, respectively. As long as both the subbands are occupied, μ increases monotonically with $|F|$. For $|F| = 9$ kV/cm, μ is about 2.7 times and 1.5 times larger in magnitude in Figs. 10 and 11, respectively compared to the value of μ at $|F| = 0$. As soon as the occupancy of second subband ceases, a sudden enhancement in μ occurs at $|F| = 10$ kV/cm. In case of Fig. 10, the enhancement in μ is around 10 times while for Fig. 11, the enhancement is 5 times the magnitude of μ at $|F| = 0$. In Fig. 10, the large enhancement in mobility is because of the displacement of the lowest subband electron wave function $[\psi_0(z)]$ away from the interface planes I_1 and I_3 due to the application of the electric field along the negative z-axis.

Normally the IR scattering dominates mobility in quantum wells having narrow well widths.[22–24] However, in Fig. 11, even for $w = 100$ Å, μ is mostly dominated by IR scattering. The dominance of IR scattering on mobility in quantum wells of larger well widths is due to the displacement of subband wave functions by applying an electric field.

We note that we have not considered the effect of alloy

FIG. 7. Scattering rate matrix elements B_{00}^{IR}, B_{11}^{IR}, C_{01}^{IR}, and D_{01}^{IR} in 10^{11} s^{-1} as a function of F along the negative z-axis.

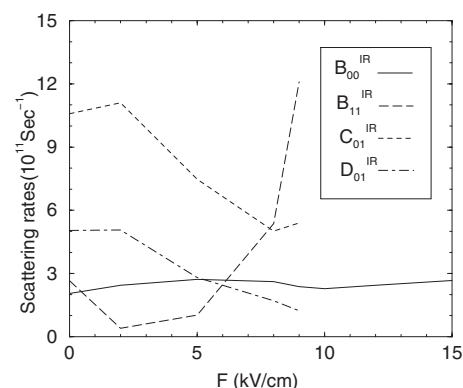FIG. 9. Scattering rate matrix elements B_{00}^{IR}, B_{11}^{IR}, C_{01}^{IR}, and D_{01}^{IR} in 10^{11} s^{-1} as a function of F along z-axis.
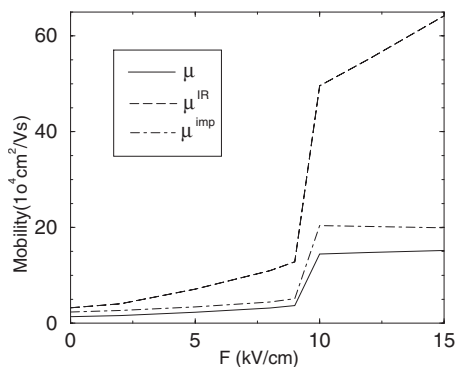
FIG. 10. Mobility due to impurity scattering μ^{imp}, IR scattering μ^{IR}, and total mobility μ in 10^4 cm^2/V s as a function of F along the negative z-axis showing the dominance of the ionized impurity scattering.

disorder scattering on mobility as this effect is small in GaInP/GaAs wells due to the small barrier height and lower alloy disorder potential.[34] The estimated contribution of the effect of the alloy disorder scatterings from the adjacent barriers and also the central barrier of the GaInP/GaAs double quantum well structure to subband mobility is less than 5%. It would be interesting to compare our results of effect of electric field on μ_i with experimental results for coupled quantum well systems, when such become available.

IV. SUMMARY

To summarize, we have made a systematic analysis of the effect of electric field on multisubband electron mobility in a Ga$_{0.5}$In$_{0.5}$P/GaAs double quantum well structure in which the side barriers are delta-doped with Si. We have studied the dependence of the intrasubband and intersubband scattering rate matrix elements on the electric field strength by considering the IR and ionized impurities scattering mechanisms. So long as two subbands are occupied, the mobility is mostly governed by the intersubband effects. At a certain applied electric field the system undergoes a transition from double subband to single subband occupancy thereby exhibiting a sudden enhancement in mobility due to vanishing of the intersubband interaction. We show that by reversing the direction of the electric field, the mobility due to ionized impurity scattering μ_i^{imp} remains unaffected because the delta-doped layers are placed symmetrically in the
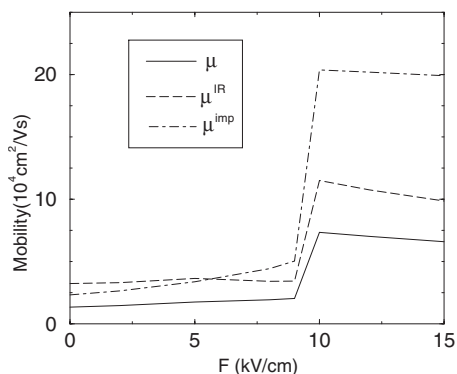
side barriers. However, the value of μ_i^{IR} varies due to the asymmetric nature of the IR potential. We note that normally the mobility is governed by the IR scattering for quantum wells of narrow well widths.[22–24] However, it is interesting to obtain the mobility dominated by the IR scattering in a quantum well of larger well widths by applying the electric field. Our analysis of the electron mobility for the coupled GaInP/GaAs quantum well system can be utilized for a variety of low temperature devices incorporating such double quantum wells.

[1]L. L. Chang, L. Esaki, and R. Tsu, Appl. Phys. Lett. **24**, 593 (1974).
[2]F. Capasso, S. Sen, F. Beltram, L. M. Lunardi, A. S. Vengurlekar, P. R. Smith, N. J. Shah, R. J. Malik, and A. Y. Cho, IEEE Trans. Electron Devices **36**, 2065 (1989).
[3]T. J. Slight and C. N. Ironside, IEEE J. Quantum Electron. **43**, 580 (2007).
[4]J. Faist, F. Capasso, D. L. Sivco, A. L. Hitchinson, and A. Y. Cho, Science **264**, 553 (1994).
[5]K. Kalna, C. Y. L. Cheung, and K. A. Shore, J. Appl. Phys. **89**, 2001 (2001).
[6]A. Wittmann, Y. Bonetti, J. Faist, E. Gini, and M. Giovannini, Appl. Phys. Lett. **93**, 141103 (2008).
[7]P. K. Basu and D. Raychaudhury, J. Appl. Phys. **68**, 3443 (1990).
[8]F. M. S. Lima, A. L. A. Fonseca, and O. A. C. Nunes, J. Appl. Phys. **92**, 5296 (2002).
[9]G. C. Crow and R. A. Abram, Semicond. Sci. Technol. **14**, 1107 (1999).
[10]Y. Zhang and J. Singh, J. Appl. Phys. **89**, 386 (2001).
[11]F. Monsef, P. Dollfus, S. G. Retailleau, H. J. Herjog, and T. Hackbarth, J. Appl. Phys. **95**, 3587 (2004).
[12]Z. Yarar, Solid State Commun. **147**, 98 (2008).
[13]R. Ferreira and G. Bastard, Rep. Prog. Phys. **60**, 345 (1997).
[14]Z. Vörös, R. Balili, D. W. Snoke, L. Pfeiffer, and K. West, Phys. Rev. Lett. **94**, 226401 (2005).
[15]M. D. Godfrey, A. Husmann, H. E. Beere, D. A. Ritchie, S. N. Holmes, and M. Pepper, J. Phys.: Condens. Matter **18**, L123 (2006).
[16]S. S. Mukherjee and S. S. Islam, Superlattices Microstruct. **41**, 56 (2007).
[17]T. Ando, A. B. Fowler, and F. Stern, Rev. Mod. Phys. **54**, 437 (1982).
[18]R. Fletcher, E. Zaremba, M. D. Iorid, C. T. Foxon, and J. J. Harris, Phys. Rev. B **41**, 10649 (1990).
[19]G. Q. Hai, N. Studart, F. M. Peeters, P. M. Koenraad, and J. H. Wolter, J. Appl. Phys. **80**, 5809 (1996).
[20]T. Sahu and J. Patnaik, J. Appl. Phys. **88**, 2658 (2000).
[21]T. Sahu, J. Appl. Phys. **96**, 5576 (2004).
[22]T. Sahu and K. Alan Shore, Semicond. Sci. Technol. **24**, 095021 (2009).
[23]S. Elhamri, A. Ahoujja, R. S. Newrock, D. B. Mast, S. T. Herbert, W. C. Mitchel, and M. Razeghi, Phys. Rev. B **54**, 10688 (1996).
[24]J. M. Li, J. J. Wu, X. X. Han, Y. W. Lu, X. L. Liu, Q. S. Zhu, and Z. G. Wang, Semicond. Sci. Technol. **20**, 1207 (2005).
[25]Y. Ando and T. Itoh, J. Appl. Phys. **61**, 1497 (1987).
[26]G. Hionis and G. P. Triberis, Superlattices Microstruct. **24**, 33 (1998).
[27]I. Dharssi and P. N. Butcher, J. Phys.: Condens. Matter **2**, 4629 (1990).
[28]P. J. Price and F. Stern, Surf. Sci. **132**, 577 (1983).
[29]R. E. Prange and T. W. Nee, Phys. Rev. **168**, 779 (1968).
[30]H. Sakaki, T. Noda, K. Hirakawas, M. Tanaka, and T. Matsusue, Appl. Phys. Lett. **51**, 1934 (1987).
[31]K. Inoue and T. Matsuno, Phys. Rev. B **47**, 3771 (1993).
[32]S. K. Lyo, J. Phys.: Condens. Matter **13**, 1259(2001).
[33]B. R. Nag, S. Mukhopadhyay, and M. Das, J. Appl. Phys. **86**, 459 (1999).
[34]B. R. Nag and M. Das, Nanotechnology **14**, 965 (2003).

FIG. 11. Mobility due to impurity scattering μ^{imp}, IR scattering μ^{IR} and total mobility μ in 10^4 cm^2/V s as a function of F along z-axis showing the dominance of IR scattering over the ionized impurity scattering.